HHS Public Access

Author manuscript

Nat Struct Mol Biol. Author manuscript; available in PMC 2017 August 20.

Published in final edited form as:

Nat Struct Mol Biol. 2017 April ; 24(4): 379–386. doi:10.1038/nsmb.3379.

HIV-Tat protein and amyloid β peptide form multifibrillar structures that cause neurotoxicity

Alina Hategan[1], **Mario A. Bianchet**[2,3], **Joseph Steiner**[1], **Elena Karnaukhova**[4], **Eliezer Masliah**[5], **Adam Fields**[5], **Myoung-Hwa Lee**[1], **Alex M. Dickens**[2], **Norman Haughey**[2], **Emilios K. Dimitriadis**[6], and **Avindra Nath**[1]

[1]Section of Infections of the Nervous System, National Institute for Neurological Disorders and Stroke, National Institutes of Health, Bethesda, MD

[2]Department of Neurology, Johns Hopkins School of Medicine, Baltimore, MD

[3]Structural Enzymology and Thermodynamics group, Department of Biophysics and Biophysical Chemistry, Johns Hopkins School of Medicine, Baltimore, MD

[4]Center for Biologics Evaluation and Research, Food and Drug Administration, Silver Spring, MD

[5]Department of Pathology, University of California at San Diego, San Diego, CA

[6]Scanning Probe Microscopy Unit, National Institute of Biomedical Imaging and Bioengineering, National Institutes of Health, Bethesda, MD

Abstract

We investigated direct interactions between the human immunodeficiency virus (HIV)-trans-activator of transcription (Tat) protein and amyloid β peptide. Amyloid β-Tat complexes are readily formed extracellularly in the brain. In vitro studies showed that in the presence of Tat, the uniform amyloid fibrils turned into double twisted fibrils followed by populations with thick unstructured filaments and aggregated large patches in a dose-dependent manner. The fibers became more rigid and mechanically resistant. Tat attached externally to fibrils, causing their lateral aggregation into thick multifibrilar structures. These present growth in β sheet and enhanced adhesion. The neurotoxic properties of Tat and amyloid β aggregates were strongly synergistic when complexed together in vitro and in animal models. These data suggest that the

Correspondence: Avindra Nath, Bldg 10; Room 7C-103, 10 Center Drive, Bethesda, MD 20892, Tel: 301-496-1561; natha@ninds.nih.gov.

DATA AVAILABILITY STATEMENT. Source data for Figures 1b,c, 2b, 4b,d,f, 5b and 6b are available with the paper online. Other data presented in the paper are available upon request.

AUTHOR CONTRIBUTIONS

A.H. and A.N. conceived of and designed the study, A.H. performed AFM, ThyT bulk fluorescence, single fibril and cell adhesion experiments, analyzed and interpreted data, M.A.B. performed the computer simulations, E.K. performed the CD measurements, J.S. performed neurotoxicity experiments, E.M. and A.F. performed the transgenic mice experiments and immunohistochemistry analysis of their brain samples, M.L. performed immunohistochemistry of the Tat-injected mice brain samples, A.M.D. and N.H. performed the Tat-injected mice experiments, E.K.D. contributed and supervised AFM data acquisition. A.H., A.N. and M.A.B. wrote the paper and all authors edited the manuscript.

COMPETING FINANCIAL INTERESTS

The authors declare no competing financial interests.

increased rigidity and mechanical resistance of the amyloid β-Tat complexes coupled with stronger adhesion due to the presence of Tat in the fibrils accounted for the increased damage, likely through pore formation in membranes.

Despite antiretroviral therapy, neurocognitive dysfunction is detected in nearly 30% of human immunodeficiency virus (HIV)-infected individuals[1] with increased incidence in older people[2,3]. HIV-infected individuals have increased deposition of amyloid β plaques in the brain[4,5]. Amyloid plaques are a hallmark of Alzheimer's disease and their role in disease pathogenesis is an area of intense investigation. Another contributing factor to neuronal injury in HIV-infected individuals may be the presence of an HIV reservoir in the brain. Even when viral replication is suppressed with brain penetrant antiretroviral drugs, HIV-trans-activator of transcription (Tat) protein can still be produced from proviral DNA[6]. Tat is released extracellularly from HIV-infected cells where it has the opportunity to interact with amyloid β peptide. Tat can also impact the production of amyloid by inhibiting its breakdown[7,8] and Tat can interact directly with amyloid precursor protein and stimulate amyloid β peptide production[9]. Here we explored if Tat can directly complex with amyloid β peptide and if it can impact its polymerization and neurotoxic properties.

Tat is a small protein composed of 86 to 101 amino acids[10]. It is the first protein to be expressed once HIV enters the cell, and is a key activator of HIV transcription[11]. Exon 1 encodes the first 72 amino acids, which constitute the most active part of the protein. The second exon defines residues 73–101, has large sequence heterogeneity and its complete biological function is not clear[12,13,14]. Structural studies of Tat in solution by nuclear magnetic resonance (NMR) performed at pH 4.1 or 6.5 predict an unstructured protein[15,16], with tendency for folding at pH 6.5[15]. The absence of a fixed conformation and the observation of fast dynamics are consistent with the ability of Tat to interact with a variety of molecules and support the concept of a natively unfolded protein[15]. A common mechanism of action for natively unfolded proteins involves partial or complete folding upon interaction with a binding partner[17]. Circular dichroism (CD) studies of Tat showed lack of secondary structure for the protein, however these tests were performed in denaturing conditions (10 mM acetate buffer at pH 4.7 [16] or at pH 4.5[18]). The crystal structure of Tat complexed with pTEFb[19] shows that, under milder crystallization conditions, the protein presents a fold or changes conformation dramatically in bound state. This active Tat bound to its target shows a well folded portion of 42 amino acids, held together by two Zn^{+2} ions and coordinated by most of the cysteine residues within the cysteine-rich region[19].

Amyloid β 1–40 (Aβ) is found in the amyloid plaques and is the most abundantly secreted amyloid peptide from the cells[20]. The structure of Aβ fibrils has been extensively studied[21] and their molecular structure, determined by solution NMR, electron microscopy or atomic force microscopy (AFM)[22–24], is largely dependent on the polymerization conditions, being significant differences between fibrils formed in quiescent or agitated conditions[22,25].

Tat can affect amyloidogenesis through several mechanisms. This includes increased production by disruption of the endolysosome[26], decreased degradation via binding to neprolysin[27], and it can also affect Aβ transport across endothelial cells through interactions with low density lipoprotein-1[28]. We present here an analysis of the direct interaction of Tat

with Aβ peptide, and determine the role of this interaction in the neurotoxicity of these complexes since both, Tat and Aβ aggregates were shown to be independently neurotoxic. We chose a combination of techniques including AFM, ThyoflavinT (ThyT) bulk and single fibril fluorescence, CD and molecular simulation to study Tat-Aβ interaction and created a model to explain their increased neurotoxic properties.

RESULTS

Tat protein increases β sheet formation and aggregation of Aβ fibrils

Our bulk measurements showed that Tat protein increased β sheet formation, aggregation of Aβ fibrils and their adherence to surfaces. CD measurements of Aβ samples showed that the predominant structure in Aβ fibrils was the β sheet, which increased in the presence of Tat (Figure 1a). Up to 20% increase in β sheet formation occured with 1.8 μM Tat and increase in β sheet was observed at all concentrations. Thyoflavin T (ThyT) bulk fluorescence measurements similarly showed increase in aggregation of Aβ peptide in the presence of Tat (Figure 1b). In contrast, bovine serum albumin inhibited Aβ aggregation at the same concentrations (Supplementary Figure 1). The Tat-Aβ complexes presented greater adhesion than Aβ to the surface of the measuring wells as evidenced by smaller ThyT signal then for measurements performed in nonbinding wells (Figure 1b). Adhesion of these complexes to the neuronal cells was also increased when Tat was present within the aggregates: larger aggregates were attached to the surface of neurons (Figure 1c) and were not removed by standard washing of the cells. The adjacent graph presents the fold increase in the size of the aggregates attached to the cells.

Tat structure and aggregation

The 1–72 aminoacids segment of Tat activates transcription with the same proficiency as the full-length protein and has a relatively conserved sequence[13,29,30]. We used this segment in our experiments. An AFM topography image of Tat 1–72 as absorbed from a phosphate buffered saline (PBS) solution at pH 7.4, onto mica surface showed that Tat exists as multi-disperse aggregates, ranging from monomers (zoom in) to large oligomers (Figure 2a). The monomer appeared as a globule, with a volume of ~ 12 nm^3, which was in agreement with the theoretical calculation of the volume based on molecular mass (Supplementary Note) and with computer simulation of the dimensions of the hydrated molecule (Supplementary Figure 2). Analysis of the distribution of sizes for Tat at pH 7.4 (Figure 2b) showed that the structures ranged from monomers, dimers and small oligomers, to 40–50-mers and larger. There seemed to be two coexistent populations, one of small oligomers and the other, more disperse, of large aggregates. Even though the monomers and dimers were more frequent than larger aggregates (for example, the sample presented here showed eleven monomers and only four 50-mers) less than 10% of the sample was in monomeric form (Figure 2b **inset**), and therefore functionally active[31]. Evaluation of the Tat secondary structure in PBS at pH 7.4 by CD was done for Tat samples at 0.1 μM, 1 μM, 10 μM, 20 μM. As shown in Figure 2c for the 10 μM sample, it exhibits three characteristic bands (208 nm, 220 nm and 194 nm) that are typical for the presence of α-helical structure. Analysis of the Tat CD data showed ~ 20% α-helical structure. It is likely that the α-helical structure represented Tat oligomers, since more than 90% of the population was in oligomeric state at pH 7.4.

Changes in the physical properties of Aβ fibril formed in the presence of Tat

AFM topography imaging showed that Aβ fibrils formed at 200 μM concentration were typically uniform along their length (Figure 3a). They were the main structures observed. At ~2500:1 ratio of Aβ peptide to Tat, a twisted fibril was the predominant structure (Figure 3b). At a ratio of 500:1, a thick irregular (along length and width) fibril was the most frequent (Figure 3c), and large aggregated patches were present at ~100:1 ratio (Figure 3d).

AFM topography imaging of a typical twisted fibrilar structure (Figure 4a) showed that the height at the top of the twist was about twice the height in the groove of the twist, whereas the groove of the twist was about the same height as the height of a typical singular fibril (Figure 4b–c), which indicates that two single fibrils were twisted together to give the twisted fibrilar structure. While the two twisting fibrils remain at their initial thickness, the distance between twists increased with Tat concentration (Figure 4d) by up to 38% at a concentration of 1.8 μM Tat. This untwisting is indicative of the mechanism that is responsible for the lateral interaction between fibrils. The lateral aggregation of amyloid fibrils is associated with hydrophobic interaction[32,33]. The untwisting of the fibrils within the twisted structure may be due to electrostatical screening of the amyloid fibrils[34]. Here, the positive charge of Tat may screen the interaction between the fibrils leading to their untwisting.

The fibrils attached to mica were rapidly dried with a compressed N_2 flow. Figure 4e shows an AFM topography image of a single Aβ fibril that ruptured under N_2 flow during the drying procedure. This indicates that these fibrils were rigid and brittle at the same time, unlike other biological fibers. With increasing Tat concentration, the distribution of rupture lengths of single fibrils shifted towards larger values, indicating increased mechanical resistance of the fibrils. The graph shows average values for the rupture lengths, which grew significantly with Tat concentration, up to 42% at 1.8 μM Tat (Figure 4f).

Tat protein binds to the external surface of Aβ fibril

The interaction between Aβ and Tat at single fiber level was determined by fluorescence microscopy. Tat conjugated to a fluorescent tag, Venus, was incubated with Aβ to form the fibrils. The fibrils were labeled with ThyT and immediately imaged. Figure 5a shows an Aβ fibril labeled with ThyT. The amount of fluorescent Tat incorporated into the amyloid fibrils increased in a dose-dependent manner (Figure 5b). We used computer simulation to visualize Tat binding to the fibrils. We modeled the structure of Tat 1–72, which was calculated by *ab-initio* threading, starting with the crystallographic structure of Tat 1–48[19] as a template. Figure 5c shows the resultant model for Tat B 1–72. The height of single Aβ fibrils obtained from high resolution AFM topography images is in agreement with the dimensions obtained by NMR for a triangular in cross-section “3 hairpins” structure of Aβ fibrils formed in quiescent conditions[25] (Figure 5d). The predicted model of Tat with the highest score (C-score: −0.9) was docked to the fibril. In Figure 5d, the first three independent solutions of the docking were superimposed. The simulation suggested that Tat binds to the external side of the hairpin, involving an interaction between a negatively charged region from the terminal regions and the hairpin turn of the Aβ molecules on one hand, and, on the other hand, positively charged residues mostly from the basic region of Tat

(Supplementary Figure 3a–c). The surface positive charge of the system Aβ-Tat increased after the binding (Supplementary Figure 3d–e). When using other tridimensional structures for Tat, obtained from solution NMR studies (1TIV, 1TBC, 1JFW, 1K5K), therefore under conditions that would affect Tat fold, the most probable binding region was still the basic region (Supplementary Figure 4). Being a very small protein, Tat amino acid sequence seemed to be more relevant than its variation in three-dimensional structure. Fluorescently labeled Tat antibody binding to Aβ-Tat fibrils showed that Tat is present on the surface of the fibrils (Supplementary Figure 5), in agreement with the binding mode suggested by the simulation.

Importantly, we found that Tat aggregates were bound to the surface of Aβ fibrils and got incorporated in the thick fibrils, as visualized by AFM (Supplementary Figure 6). The computational analysis was restricted to the Tat monomer, although the interaction of Tat oligomer might utilize a mechanism similar to the monomer case.

Aβ–Tat fibrils have increased neurotoxicity

Cultures of fluorescently labeled rat hippocampal neurons were exposed to Aβ–Tat fibrils and compared to the effect of regular Aβ fibrils. Images of neurons after 48 hours exposure are shown (Figure 6a). Increasing Tat concentration in the Aβ-Tat complexes resulted in more neuronal damage (Figure 6b) as evidenced by decreasing neuronal cell count, reduced mean neurite lengths in the remaining neurons and the appearance of puncta along neuronal processes. When neurons were exposed to only Tat, incubated in PBS similarly for 7 days at room temperature, no significant toxicity was observed (Supplementary Figure 7). Further, freshly prepared Tat at 180 nM did not induce significant neuronal damage (Supplementary Figure 7). Tat neurotoxicity at these concentrations and incubation times was much lower than the neuronal damage induced by Aβ or Aβ-Tat complexes (amyloid precursor protein-presenilin1: APP-PS1). To determine if Aβ-Tat complexes can occur *in vivo*, we initially injected Tat into the brain of a well characterized transgenic mouse model of Alzheimer's disease known to form amyloid plaques. We found that the Tat protein was localized to the amyloid plaques (Figure 7a). We next generated APP-Tat double transgenic mice and found that Tat colocalizes with APP in the brains. The Tat-amyloid complexes were present both inside the neurons, mainly in the granular structures (Figure 7b), and outside of the neuronal cells (Figure 7c). This data confirms that the Tat protein has specific avidity for Aβ in the brain and animals with the Aβ-Tat complexes had increased evidence for neurodegeneration. Additional pathological features in the transgenic mice are presented in Supplementary Figure 8.

DISCUSSION

Since Tat is released extracellularly from HIV-infected cells and amyloid plaques are present in increasing amounts extracellularly in the brain of HIV infected individuals, we investigated if the two proteins may interact with one another. We found that Tat protein localizes to the amyloid plaques within the brain of APP-PS1 transgenic mice. Hence we investigated the biophysical properties of Tat-Aβ interaction with bulk methods and then using techniques with fibrilar and molecular resolution. Our main finding is that, at pH 7.4,

Tat has significant molecular interaction with Aβ, resulting in major changes in its physical and functional properties.

We studied the Tat structure at pH 7.4 in PBS, by using AFM high resolution imaging to characterize the size of the monomers and oligomers, and their distribution. AFM showed that Tat has a compact globular structure. Tat has a remarkable ability to form oligomers and we found that more than 90% of the protein was in an oligomerized state. Some oligomers were large, being formed of more than 50 molecules of Tat. The monomeric Tat assumed a globular structure, as expected for a small, unstructured protein, and the multimeric forms of Tat maintained the globular shape. The spherical shape allows Tat to assume the least possible volume, at the lowest free energy state. The oligomerized state is believed to be functionally inactive[31]. This would suggest that Tat may be nearly 10 fold more potent as a neurotoxin than suggested by the *in vitro* assays[35,36]. The role of oligomers in the neuropathogenesis of HIV infection remains unclear, however was shown that oligomerized Tat can be taken up by lymphocytes resulting in activation of these cells[6]. Here, we found that Tat oligomers can bind to amyloid fibrils (Supplementary Figure 6) adding significant electrostatic charge to the Aβ, thus providing another functional role for the oligomers.

Our CD measurements showed that, in an aggregated state, Tat changed conformation towards a more ordered state: α helix. NMR studies suggest that the most likely region to fold into a secondary structure is the Cys-rich region[15]. Cys-Cys interactions are also involved in oligomerization[28] suggesting that the α–helix structure seen by CD might be due to the Cys region of the protein.

We found that the growth of Aβ fibrils is enhanced in the presence of Tat. Both β sheet formation leading to elongation of fibrils and lateral aggregation of elongated fibrils, increased significantly. One of the structures observed was the double twisted fibril (Figure 4). Amyloid fibrils of denatured β lactoglobulin show similar structures, involving 2, 3 and 4 fibrils twisted together[37]. In contrast, twisted fibrils of Aβ and Aβ-Tat contained only two fibrils. Aβ fibrils are rigid structures (2–4 GPa[38]). The distance between the twists in the twisted fibrilar structures increased with Tat concentration, providing insights into the mechanism of lateral aggregation of the Aβ-Tat fibrils. We observed untwisting of the fibrils, due to the electrostatic screening of the forces between them, induced by the positive charge of Tat. As shown by computer simulation, Tat, once bound to the fibril, is capable of further interaction, and therefore can electrostatically bridge the amyloid fibrils at the same time. The lateral aggregation of these fibrils is likely to be due to a superposition of hydrophobic and electrostatic interactions between the fibrils and Tat.

We showed that Aβ fibrils broke under N_2 flow, and their mechanical resistance increased with Tat in the fibril. At higher Tat concentrations the fibrils become larger, thicker and irregular along their height and width. Increase in the thickness of amyloid fibrils is related to increase in their rigidity[39]. It was shown before that amyloid fibrils distort cell membranes and induce rupture[40] due to their stiffness, as crucial factor[41]. The neurons are several orders of magnitude softer (52–308 Pa)[42] therefore the larger, thicker, and more rigid Aβ-Tat aggregates would be more likely to damage the neuronal cell membrane compared to Aβ fibrils alone.

Our computer simulation suggested that Tat, using the basic region, bound to the negatively charged patch at the external side of the Aβ fibrils, near the junction between the Aβ molecules (Supplementary Figure 3). In accordance, we found that more and much larger Aβ aggregates attached to neurons when Tat was present in the aggregates as a consequence of Tat presence on the surface of fibrils. This accounted for stronger binding to membranes. It is known that small aggregates of Aβ peptide are more toxic than long fibrils[43]. Therefore, a molecule that increases aggregation will reduce neurotoxicity[43]. In contrast, we found that Tat, a small peptide, increased aggregation of Aβ and at the same time, dramatically increased degeneration and neuronal death. Tat protein loses its neurotoxic potential rapidly by aggregation and oxidation[31]. However, in the presence of Aβ peptide even after seven days at room temperature under atmospheric conditions the toxicity of Aβ-Tat aggregates were enhanced, as compared with Aβ only.

Amyloid aggregation can be manipulated with small molecules[43], some accelerating fibrilogenesis[44], some blocking it[45]. Bovine serum albumin inhibits fibril formation and this results in increased neurotoxicity[46]. We observed this even at the low concentrations used for Tat (Supplementary Figure 1). Therefore Tat was unusual, since it increases both aggregation and neurotoxicity at the same time.

The mechanism of Aβ toxicity on neurons has been studied extensively and it has been shown that Aβ interacts directly with the cell membranes[47, 48] via charged lipids in the membranes, to induce oxidative stress[49]. Aβ can also activate astrocytes and microglia to kill neurons[50]. Aβ aggregates bind strongly to the cell membranes[47, 48]. We found even stronger binding when Tat was present in the aggregates (Figure 1c), as expected, since Tat in known to bind to several receptors on the cell membranes[10]. Irrespective of Tat functionability in these complexes, it did bring positive charge on the surface of fibrils, which contributed towards stronger passive adhesion[51,52] of aggregates to the membrane. It has been shown previously that strong passive adhesion to a positively charged surface induces reorganization of the membrane proteins, cytoskeletal proteins, and also lipid migration in the contact area, which leads to tension in the membrane and it's rupture[53]. In addition, the positively charged Arginine-rich region of Tat interacts with the negatively charged phospholipids in the cell membrane inducing a curvature in the lipid regions, which results in pore formation[54]. We directly observed lysis of neurons during the first 15 minutes of exposure to Aβ-Tat complexes (Supplementary Figure 9) whereas no lysis was observed when neurons were exposed to Aβ alone in the same time frame.

Based on the bulk data, molecular structure of single fibrils and aggregates and on the computer simulated interaction we propose a model of interaction of Aβ with Tat protein that may account for the increased neurotoxicity of the complexes. The proposed model consists of two pathways. The minor pathway proposed involves small Aβ–Tat aggregates, which were in reduced number, since the Tat induced large aggregation of Aβ peptide. Being a membrane penetrating molecule, Tat attached to small aggregates is likely to succeed in entering the cells with the Aβ "cargo", to induce damage. In particular, the segment between Tyr-47 and Arg-57 of Tat has been used to transport a variety of materials across cell and nuclear membranes[55]. However the predominant species in Aβ–Tat complexes were the large aggregates. The major pathway we propose involves these predominant large Aβ–Tat

complexes (Figure 8). Accordingly, Tat attaches to the surface of a typical Aβ fibril (Figure 8a). At small concentrations of Tat, it binds to the surface of the fibrils which randomly come close to each other in solution and then twist around each other to form a double fibril (Figure 8b). At higher concentrations of Tat, more fibrils, long and short, attach to each other to form irregular thick fibrils (Figure 8c). Further increase in Tat concentration leads to aggregation of these fibrils resulting in large patches (Figure 8d). These thick structures are more rigid and have increased adherence to neurons due to the known binding capacity of Tat to membranes[10] (Figure 8e). In the contact region, at the edge of the attached plaque or fibril to the membrane, shear forces appear due to the normal dynamic fluctuations of the membrane near a rigid surface[56], and can induce pore formation and eventually rupture of cell membrane. Tat is a highly positively charged molecule[16]. Although the majority of these positive charges are predicted by computer simulation to participate in the interaction with the Aβ fibril negatively charged patch, a number of them also are predicted to remain exposed (Supplementary Figure 3a–c), therefore available to interact further with the membrane. The Tat aggregates that are bound to the Aβ-Tat complexes (Supplementary Figure 6) bring additional significant positive charge to fibrils. The additional positive charge can induce a strong adhesion regime[51, 52]. In this regime, only due to the positive charges, lipids migrate in the contact region between the hard surface (the Aβ-Tat complex) and the membrane and proteins are reorganizing in the contact region[51] inducing tension in the remaining membrane, which leads to pore formation and rupture[51]. Since Tat concentrations used did not induce significant neurotoxicity by themselves (Supplementary Figure 7) it is likely that mainly the charge added to the Aβ fibrils by Tat monomers and oligomers is responsible for the changes. Additionally, the capacity of Tat to bind to specific receptors in the membrane[10] would increase the contact strength between the membrane and the rigid Aβ–Tat fibrils.

While our study was performed at pH 7.4, Aβ genesis occurs in acidic organelles in neurons. In vitro studies show that Tat can be taken up, including with cargo, into cells[55]. However, immunostaining of brain tissue from HIV-infected patients show Tat in perivascular macrophages and microglial nodules, but not in neurons[6,57]. These observations lead us to conclude that when Tat is released extracellularly, it aggregates in extracellular compartments and if there is extracellular Aβ, it binds preferably to it. The smaller fraction of Tat molecules that may remain unbound might enter other cells. Figure 7 shows colocalization of Tat and Aβ in extracellular aggregates and in some neurons of the double transgenic mice. This is consistent with the possibility that small Aβ-Tat aggregates may enter the neurons from the extracellular compartment as presented in our model in Figure 8. Previous studies have shown that Aβ aggregation is enhanced at lower pH and is more cytotoxic[58]. The production of Aβ is further enhanced by exposure of neurons to Tat which also results in disruption of the endolysosome[26]. The events at more acidic pH, at the endolysosome level, might be relevant for cell malfunction and death, however the more significant damage would occur in time to the neighboring cells since once the cell is damaged, the aggregates are released extracellularly where they may reside long time or almost indefinitely at pH 7.4. This provides justification for our studies at pH 7.4.

In conclusion, we constructed a model that explains the formation of the Aβ-Tat complexes and their increased neurotoxicity, based on possible penetration of the few small aggregates

through the cell membrane, and, as a major pathway towards cell damage, a model based on the increased adherence of the predominant large, positively charged Aβ–Tat complexes to membranes and on the induced mechanical disruption of membranes, which is caused by the large difference in stiffness between the neurons and the rigid Aβ-Tat complexes and by the Tat-induced local reorganization of the membrane.

ONLINE METHODS

Materials

Aβ peptide was purchased from Bachem, Bubendorf, Switzerland (catalog number: H 1194), ThyT was obtained from Sigma-Aldrich, St. Louis, MO, USA (catalog number: T3516-5T), FITC antiTat antibody was purchased from Abcam, Cambridge, MA, USA (catalog number: ab43016), TatVenus (Tat tagged with a mutated form of GFP called Venus) was produced in our laboratory[59]. AFM probes OTESPA were purchased from Bruker, Camarillo, CA, USA. For the Tat-injected experiment, mouse anti-HIV Tat antibody was purchased from Biolegend, San Diego, CA, USA (catalog number: 919001), rabbit anti-APP antibody from Abcam, Cambridge, MA, USA (catalog number: ab2072). Secondary antibodies, Alexa Fluor 488 goat anti-mouse IgG (catalog number: A11029) and Alexa Fluor 594 goat anti-mouse IgG (catalog number A11012) were obtained from Invitrogen, Grand Island, NY, USA. For the second mice experiment, the antibody against Aβ (4G8) was purchased from Sigma-Aldrich (catalog number A1349). The mouse monoclonal antibody against HIV-Tat was from NIH AIDS reagent program (catalog number 1974). The secondary antibodies used were FITC-tagged anti-mouse antisera and the tyramide red amplification system (Thermo-Fisher Scientific catalog number B40957) for Tat detection. The superfrost slides used were from Fisher (catalog number 12–550-15). The Wizard genomic DNA isolation kit was from Promega, Madison, WI. Doxycycline was purchased from Sigma-Aldrich.

Preparation of Tat

Recombinant Tat (1–72) was prepared using column chromatography as previously published[60]. Protein was produced in an endotoxin free manner and was greater than 95% pure as determined by gel electrophoresis and Western blot analysis. Stocks of 0.2 μg/μl were stored at −80°C until used.

Preparation of Aβ fibrils

The lyophilized Aβ powder was dissolved in ultrapure water to 1 mM concentration and immediately vortexed for 1 minute before diluting further in PBS to 200 μM concentration, which was used for growth of fibrils in quiescent conditions. The samples were incubated at room temperature for 7 days, in the presence of various concentrations of Tat. As observed by both AFM and ThyT fluorescence imaging, most of the fibrils were relatively short, in the range of up to 1–2 μm. Therefore for the experiments of single fibrils fluorescence imaging, the method of Ban et al.[61] was used to prepare long fibrils by seeded growth. Briefly, Aβ monomers[61] at 50 μM were mixed with 25 μM seeds (Aβ aggregates sonicated for 1 min) and incubated for 7 days at room temperature.

AFM imaging—was performed with a Multimode Atomic Force Microscope (Brucker). The stock Tat solution was diluted 100 times in PBS, centrifuged at 16000g for 30 min to eliminate the very large aggregates, then diluted further in PBS to 5 nM concentration. Aliquotes of 10 μl of this were allowed to adsorb for 5 min on clean freshly cleaved mica surfaces. Each mica surface was subsequently washed with PBS (2 X 200 μl) and pure water (5 × 100 μl) to avoid salts crystal formation on the surface and the samples were dried in N_2 flow. In order to image the Aβ-Tat samples, 10 μl of the incubated fibrils were allowed to adsorb for 5 min on mica surface, then they were washed as in the case of Tat samples and dried in N_2 flow. Imaging was performed in air in tapping mode with oxide sharpened AFM tips (OTESPA), that have a nominal spring constant of 42N/m. Scanning was performed with a scanning rate of 1 Hz. Data analysis of the Tat particles present in the topography images was done as presented in Supplementary Note. The height measurements in the images of Aβ and Aβ-Tat complexes were performed with the Nanoscope software. The images were flatten before the height measurements. The lengths of Aβ fibrils were determined at half height. At least two independent experiments were used in the study of Aβ and Aβ–Tat complexes.

Circular dichroism

Far-UV CD spectra were recorded with a Jasco J-815 Spectropolarimeter (JASCO Co., Japan) at 25±0.2 °C maintained by a Peltier temperature controller (JASCO). The CD spectra were recorded in 0.05 cm path length quartz cuvettes (Starna, Inc.) from 300 nm to 180 nm using a scan speed of 100 nm/min, bandwidth of 1.0 nm and resolution of 0.2 nm, and accumulated in a triplicate. All samples were prepared and measured in PBS, pH 7.4. The baseline was subtracted by running PBS as a blank prior to the sample solutions. For time course CD measurements of Aβ–Tat complexes, the samples were incubated for seven days at room temperature in the measuring cuvettes to avoid possible impact of the pipetting on ongoing structural alteration. An ellipticity of CD spectra was expressed in millidegrees (mdeg). To evaluate the secondary structure of Tat preparations, the CD spectra of freshly prepared Tat solutions in PBS were converted into a mean residual molar ellipticity, and analyzed by using CDPro/CONTIN software (SP43). Four independent experimets were measured in CD.

Fluorescence bulk ThyT measurements—were performed spectrofotometrically by using a FlexStation3 plate reader (Molecular Devices) equipped with SoftMaxPro software. ThyT solution at a concentration of 5 μM in PBS was filtered prior to use, by using a Millex-GS 0.22 μm syringe filter. For the measurement, 9 μl of each Aβ or Aβ–Tat sample was added to 375 μl of ThyT solution and 125 μl of this mix was introduced in each of the plate wells for measurements. Excitation wavelength used was 440 nm and emission was measured at 485 nm with an automatic cut-off filter set at 475 nm. The standard plates (wells) used were Costar 3631, the low binding plates (wells) were Corning 3651, and the experiments were performed in parallel. The Corning 3651 low binding plates had a modified polymer surface that resulted in a non-ionic hydrophilic surface that minimized molecular interactions - a trademark of Corning. Several independent experiments were done for both incubation in vial and incubation in plates of Aβ-Tat complexes.

Single fibril imaging—was performed with a Nikon Eclipse Ti total internal reflection fluorescence (TIRF) microscope equipped with a 488/561/405/647 LU4A Lasers System, and an Andor iXon3 EMCCD camera by using an APO TIRF 100X NA 1.49 objective. Images were acquired with NIS-Elements AR software. We incubated TatVenus with Aβ for seven days, according to a standard procedure of forming fibrils[61], and then observed the localization of Tat at the fibrils level. Exposure time for the TIRF images was 20 ms at a 2% 488 nm laser power. The Aβ fibrils were identified by ThyT fluorescence by imaging simultaneously with the same system, with an exposure time of 10 ms at a 75% power of an X-cite fluorescence lamp / Lumen Dynamics. For this, ThyT was added to the formed fibrils before imaging, since its hydrophobic binding to the fibrils β sheet makes the fibrils visible in fluorescence microscopy[61]. The TatVenus signals were reported relative to the ThyT signal for each fibril in order to quantify the increase of TatVenus per fibril unit area. Two independent experiments were performed, with similar results.

Neurotoxicity experiments

Sprague Dawley rat hippocampal neuronal cell cultures free of mycoplasma were used *in vitro*. For this, the rat embryos were euthanized at gestation day 18 and their hipocampi and cortices harvested and used to generate the neuronal cellular cultures (IACUC protocol nr. 1330-14). The cells were plated in 96-well plates at a density of 4×10^5 cells per ml. This mixed rat neuronal culture consisted of 40–45% β-III tubulin expressing neurons, 50–55% GFAP expressing astrocytes and about 1% microglia[62]. Rat neuronal cultures were transfected with β-III Tubulin-td Tomato fusion protein driven by the CamKII promoter and plated at 40,000 cell/well on a 96 well plate. These neuronal cultures were allowed to differentiate for 12–17 days prior to treatment with Aβ or Aβ–Tat complexes, which were prepared as described. By applying the Aβ and Aβ–Tat complexes to the wells, their final concentration in the wells (therefore on the neurons) was 10 times reduced (to 8 nM, 40 nM or 180 nM for Tat in complexes and to 20 μM Aβ), however the fibrils and complexes were already formed and active, and these are not the “fibril formation” concentrations, but inform on the amount of material in the wells. Live cell imaging of the neuronal cultures was accomplished after 24, 48 and 72 hours of exposure with 10X magnification on the GE INCell Analyzer 2000 imager, acquiring images of four fields per well at each time point. GE Developer Toolbox was used to quantitate neuronal cell number, neurite length, and neuronal degradation puncta from neuronal cultures that contained tdTomato fluorescence throughout these cells. These fluorescent images were segmented, and analyzed at a medium sensitivity setting of 60. Visual inspection of 10–12 random images showed that we captured and measured more than 95% of the fluorescently labeled cells in these fields. At least four independent experiments were performed for neurotoxicity tests.

Cell adhesion experiments

Rat neuronal cell cultures as presented in *Neurotoxicity experiments* section were allowed to attach to the poly-lysine coated glass of MatTek Petri dishes in order to form a uniform layer of cells. The neurons were treated with Aβ or Aβ–Tat complexes, which were prepared as described. The complexes were allowed to attach for 2 hours, then the unbound structures were washed away twice with cell media. A 2 μM ThyT containing cell media was added on cells to signal the presence of Aβ complexes. After 2 min the cells were washed with PBS

and imaged with the system presented in *Single fibril imaging* section. Exposure times were10 ms for the ThyT (CFP channel) and 50 ms for the tdTomato (TRITC channel) at a75% power of the X-cite fluorescence lamp. Three independent experiments were performed for the adhesion experiments.

Immunohistochemistry and confocal microscopy of transgenic mice brain samples

Two independent experiments were performed, in two different labs. Animals were not randomized to groups. In the first experiment, six-month-old transgenic C57BL-6 mice expressing mutations in human amyloid precursor protein (APP_{SWE}; K670N/M671L) and human presenilin 1 (PS1; dE9) were used in these studies. APP-PS1 mice express APP and PS1 under the control of prion promoters[63]. They were maintained as a heterozygote genotype. Mice were housed in an animal facility on a 12 hours light/dark cycle with *ad libitum* access to food and water. All procedures were conducted in accordance with NIH guidelines for the Use of Animals and Humans in Neuroscience Research and approved by Institutional Animal Care and Use Committee (Johns Hopkins University School of Medicine, protocols number M015 and M268). Recombinant Tat1–72 protein was stereotaxically injected (0.5 μl/10μg in saline) into the frontal cortex (bregma, AP + 1.5 mm, ML −1 mm, DV + 1 mm)[64] and the hippocampus (AP −2 mm, ML −1.2 mm, DV + 1 mm, + 2 mm)[64]. Mice were sacrificed one week (n=2) or two weeks (n=2) following Tat injections. Animals were deeply anesthetized with isofluorane and perfused transcardially with saline followed by 4% (w/v) paraformaldehyde. After post-fixing in paraformaldehyde overnight, brains were immersed in a 30% (v/v) sucrose solution. On the following day, brains were cryoprotected and cut in the coronal or horizontal plane into 40 μm thick sections on a sliding microtome. Sections were washed in Tris-Buffered Saline (TBS) (10 mM Tris-HCl, 150 mM NaCl, pH 7.5). Tissues were incubated in blocking solution (TBS with 0.5% (v/v) Triton-X and 2.5% (v/v) donkey serum). Primary antibodies were diluted in blocking solution as follows: mouse anti-HIV Tat 1:500 and rabbit anti-APP 1:500, before use. Secondary antibodies used (conjugates of Alexa Fluor 488 or Alexa Fluor 594) were diluted 1:250 before use and the procedure was followed by washing the tissues and counterstaining with DAPI to label the nuclei. The images were obtained using a LSM 510 META laser-scanning confocal microscope (Carl Zeiss, Jena, Germany) equipped with a 63X Plan–Apo/1.4 NA oil objective. Tat imaging was done by using the 488 nm channel with 20% laser power and AAP imaging by using the 561nm channel at 20% laser power. Analysis was done in an unblinded manner. In the second experiment, mice expressing human APP751 cDNA containing the London (V717I) and Swedish-(K670M/N671L) mutations under the regulatory control of the murine (m)Thy-1 gene (mThy1-hAPP751, line 41)[65] were used. These mice display early amyloid deposition, behavioral deficits, and degeneration of the limbic and cholinergic systems[66]. These APP transgenic mice were then cross-bred with inducible Tat transgenic mouse colonies that were obtained by generation of two separate transgenic lines Teton-GFAP mice and TRE-Tat86 mice, and then cross-breeding of these two lines of transgenic mice as previously described[67]. Founder animals and progeny carrying the transgenes were identified by PCR analysis of genomic DNA, which was extracted from mouse tail clippings (0.5 to 1 cm long) using the Wizard genomic DNA isolation kit. The Tat transgene was induced by treatment with doxycycline for 2 weeks at 80 mg/kg daily intraperitoneal injections as previously described[67]. A total of n=8

non-transgenic and n=8 APP/Tat transgenic mice were generated, with ages between 4 to 6 months. All following procedures were conducted in accordance with NIH guidelines for the Use of Animals and Humans in Neuroscience Research and approved by the University of California at San Diego Animal Subjects Committee (protocol number S02221). Mice were anesthetized with chloral hydrate and flush-perfused transcardially with 0.9% saline. Brains from non-transgenic (n=8), Tat transgenic (n=4), APP transgenic (n=4) and APP-Tat transgenic (n=8) were removed and divided in sagittal sections. The right hemi-brain was post-fixed in phosphate-buffered 4% PFA (pH 7.4) at 4 °C for 48 h for neuropathological analysis, while the left hemi-brain was frozen and stored at −70°C for subsequent RNA and protein analysis. Immunohistochemical analysis was performed using free-floating, 40 μm-thick, vibratome-cut, blind-coded sections. Briefly, sections were incubated overnight at 4 °C with antibodies against Aβ (4G8) and Tat (mouse monoclonal antibody against HIV-Tat). Sections were then reacted with secondary antibodies tagged with FITC to detect Aβ and with the tyramide red amplification system to detect HIV-Tat protein. Sections were mounted on superfrost slides and coverslipped with media containing DAPI. Sections were imaged with a Zeiss 63X (N.A. 1.4) objective on an Axiovert 35 microscope (Zeiss, Germany) with an attached MRC1024 laser scanning confocal microscope system (BioRad, Hercules, CA). The imaging was done at 900× laser power by using the red channel (excitation 596 nm/emission 615 nm) and green channel (excitation 490 nm/emission 525 nm). All analysis was done after blinding the investigator to the groups of animals.

Computer simulation

In order to perform the docking of Tat to the Aβ fibril, first was created an Aβ fiber model consisting of twelve 3-hairpins spanning at least 1.5 times the longest linear dimension of the Tat structure (which is to be used as the docking target in the simulation). This model was made by elongating in the direction of the fiber main axis the triangular structure of the Aβ fibrils grown in quiescent conditions (2LMQ model 1)[25]. Briefly, the protocol used to make this elongated model was: the mathematical transformation between two consecutive 3-hairpins in the fiber was applied iteratively to the fiber-end hairpin to generate a new 3-hairpin element growing the fiber along its main axis. The transformation and coordinates of the new hairpin element were obtained with the molecular modeling program O[68]. We did not attempt to model the highly flexible Aβ N-terminal region (amino acids 1–8) in our docking simulation because of the large non-favorable entropic contribution expected by the participation of highly flexible regions in protein-protein interactions. Even though it would contribute to the binding, to make it stronger, this small region, being highly flexible, is expected to have a small favorable free energy contribution. We chose not to use the 2M4J structure of 1–40 Aβ fibril determined from a single patient[69], since more research into the variability between structures found in patients is needed before using one or the other structure as the most probable structure formed in vivo[69] and, this structure in particular was found to be unstable, by computer simulation[70]. We chose the 2LMQ structure for the fibrils formed in vitro to be the one to characterize the fibrils that we used experimentally to interact with Tat, as they were prepared in the same way.

The unobserved C-terminal region of Tat in the crystallographic structure[19] contains most of the positively charged residues. To include this relevant region, and complete the partial

crystallographic structure of Tat (3MI9 model 1), an *ab-initio* threading of the unobserved C terminal region (amino acids 49–72) was performed using I-Tasser server[71] with the default parameters (Figure 5c). We found the crystallographic structure for Tat to be the closest representation of our active Tat, since our force spectroscopy experiments indicated alpha helical structure within the Tat monomer at pH 7.4 (data not shown), in a 44 amino acids long region on average, in good agreement with the crystalographic structure. Additionally, the crystalographic structure was obtained in milder conditions than the other structures available in the protein data bank (which were NMR derived, at low pH and in an extreme high reducing environment). The resulting hybrid model of Tat with the highest score (C-score: −0.9) calculated by I-Tasser[71] was docked to the fibril using ClusPro (version 2; http://cluspro.bu.edu)[72]. A typical simulation run generates 1000 docking solutions ranked by the strength of the interaction with the target. It was used fast Fourier Transform based rigid docking, solution clustering, and, to remove clashes, minimization using a CHARMM force-field as is implemented in the ClusPro server. The first three docking solutions were presented (Figure 5d, Supplementary Figure 3). The solutions obtained by displacement along fibril axis and the three-fold symmetry around the axis were discarded by inspection, being considered not independent. The in-solution NMR structures of Tat, (obtained at low pH and under denaturing reducing conditions, therefore in conditions known to reduce the fold) were docked as well to observe if there are changes in the binding. All the simulations using different Tat structures obtained from the protein data bank (the first model of each 1K5K, 1JFW, 1TIV, and 1TBC) cluster almost all of the higher score docking solutions in the junction region of the 3-hairpins with few docking solutions at the external side of the 3-hairpin (Supplementary Figure 4). All the programs used in computer simulation are freely available on the web, as reported here, in Supplementary Note and in references.

Statistics

Data presented in Figure 1b was analysed by an unpaired Student's T test. Data presented in Figures 1c, 4b,d,f, 5b and 6b was analysed using one way ANOVA with Fisher's comparison test by using Origin 9 software. All statistical tests were two-tailed. In Figure 1b, Student's T test gave at 0.4 μM concentration $p<0.05$ with t statistic −2.8221 and degrees of freedom (DF) 22 and at 1.8 μM concentration $p<0.05$ with t statistic −2.07912 at equal variance assumed and DF 22. In Figure 1c, ANOVA with Fisher's comparison test gave $p<0.0001$ with F 11.72974 and DF = DF_{model} + DF_{error} = 118. In Figure 4b, ANOVA with Fisher's comparison test gave for the top of the twists $p<1E-6$ with F 62.22741 and DF = 63 and for the case of grooves heights and singular fibrils heights non-significance at $p<0.5$ level. In Figure 4d, ANOVA with Fisher's comparison test gave $p<0,05$ and $p<0.001$ with F 17.07921 and DF=140. In Figure 4f, ANOVA with Fisher's comparison test gave $p<0.05$ and $p<0.001$ with F 5.4276 and DF 173. In Figure 5b, ANOVA with Fisher's comparison test gave $p<0.001$ and $p<1E-6$ with F 13.70386 and DF=64. In Figure 6b, ANOVA with Fisher's comparison test gave in the neuronal cell count graph $p<0.01$ and $p<1E-6$ with F 11.02609 and DF=127, in the neurite lengths graph $p<0.001$ and $p<1E-6$ with F 10.72544 and DF=125 and in the puncta graph, $p<1E-6$ with F 23.18199 and DF=123.

Supplementary Material

Refer to Web version on PubMed Central for supplementary material.

Acknowledgments

We thank M. Bachani for preparing the Tat protein stocks, K. Mather for preparing the neuronal cell cultures used in the adhesion imaging experiments, and A. Savonenko from Johns Hopkins University School of Medicine, Baltimore MD for providing the APP-PS1 mice. This work was supported by intramural funds from NINDS, NIH: Z01-NS003130 for A.N., E.M. was supported by NIH grant R01-AG005131, N.H. was supported by grant R01-MH096636 and E.K.D. was supported by Z01-EB000085.

REFERENCES

1. Heaton RK, et al. HIV-associated neurocognitive disorders before and during the era of combination antiretroviral therapy: differences in rates, nature, and predictors. J. Neurovirol. 2011; 17:3–16. [PubMed: 21174240]
2. Valcour VG, Shikuma CM, Watters MR, Sacktor NC. Cognitive impairment in older HIV-1-seropositive individuals: prevalence and potential mechanisms. AIDS. 2004; 18:S79–S86. [PubMed: 15075502]
3. Becker JT, Lopez OL, Dew MA, Aizenstein HJ. Prevalence of cognitive disorders differs as a function of age in HIV virus infection. AIDS. 2004; 18:S11–S18. [PubMed: 15075493]
4. Esiri MM, Biddolph SC, Morris CS. Prevalence of Alzheimer plaques in AIDS. J. Neurol. Neurosurg. Psychiatry. 1998; 65:29–33. [PubMed: 9667557]
5. Green DA, et al. Brain deposition of β-amyloid is a common pathologic feature in HIV positive patients. AIDS. 2005; 19:407–411. [PubMed: 15750394]
6. Johnson TP, et al. Induction of IL-17 and nonclassical T-cell activation by HIV-Tat protein. Proc. Natl. Acad. Sci. USA. 2013; 110:13588–13593. [PubMed: 23898208]
7. Pulliam LJ. HIV regulation of amyloid β production. Neuroimmune Pharmacol. 2009; 4:213–127.
8. Daily A, Nath A, Hersh L. Tat peptides inhibit neprilysin. J. Neurovirol. 2006; 12:153–160. [PubMed: 16877296]
9. Kim J, Yoon JH, Kim YS. HIV-1 Tat interacts with and regulates the localization and processing of amyloid precursor protein. PLoS One. 2013; 11:e77972.
10. Debaisieux S, Rayne F, Yezid H, Beaumelle B. The ins and outs of HIV-1 Tat. Traffic. 2012; 13:355–363. [PubMed: 21951552]
11. Bagashev A, Sawaya BE. Roles and functions of HIV-1 Tat protein in the CNS: an overview. Virol. J. 2013; 10:358–378. [PubMed: 24359561]
12. Guo X, et al. Suppression of an intrinsic strand transfer activity of HIV-1 Tat protein by its second-exon sequences. Virology. 2003; 307:154–163. [PubMed: 12667823]
13. Smith SM, et al. An in vivo replication-important function in the second coding exon of Tat is constrained against mutation despite cytotoxic T lymphocyte selection. J. Biol. Chem. 2003; 278:44816–44825. [PubMed: 12947089]
14. Avraham HK, Jiang S, Lee TH, Prakash O, Avraham S. HIV-1 Tat-mediated effects on focal adhesion assembly and permeability in brain microvascular endothelial cells. J Immunol. 2004; 173:6228–6233. [PubMed: 15528360]
15. Shojania S, O'Neil JD. HIV-1 Tat is a natively unfolded protein: the solution conformation and dynamics of reduced HIV-1 Tat-(1–72) by NMR spectroscopy. J. Biol Chem. 2006; 281:8347–8356. [PubMed: 16423825]
16. Shojania S, O'Neil JD. Intrinsic disorder and function of the HIV-1 Tat protein. Protein Pept. Lett. 2010; 17:999–1011. [PubMed: 20450479]
17. Uversky VN. Natively unfolded proteins: a point where biology waits for physics. Protein Sci. 2002; 11:739–756. [PubMed: 11910019]
18. Mediouni S, et al. Identification of a highly conserved surface on Tat variants. J. Biol. Chem. 2013; 288:19072–19080. [PubMed: 23678001]

19. Tahirov TH, et al. Crystal structure of HIV-1 Tat complexed with human P-TEFb. Nature. 2010; 465:747–751. [PubMed: 20535204]
20. Sisodia SS, Koo EH, Beyreuther K, Unterbeck A, Price DL. Evidence that beta-amyloid protein in Alzheimer's disease is not derived by normal processing. Science. 1990; 248:492–495. [PubMed: 1691865]
21. Ball KA, Wemmer DE, Head-Gordon T. Comparison of structure determination methods for intrinsically disordered amyloid-β peptides. J. Phys. Chem. B. 2014; 118:6405–6416. [PubMed: 24410358]
22. Petkova AT, et al. Self-propagating, molecular-level polymorphism in Alzheimer's β-amyloid fibrils. Science. 2005; 307:262–265. [PubMed: 15653506]
23. Kodali R, Williams AD, Chemuru S, Wetzel R. Abeta(1–40) forms five distinct amyloid structures whose β-sheet contents and fibril stabilities are correlated. J. Mol. Biol. 2010; 401:503–517. [PubMed: 20600131]
24. Moores B, Drolle E, Attwood SJ, Simons J, Leonenko Z. Effect of surfaces on amyloid fibril formation. PLoS One. 2011; 6:e25954. [PubMed: 22016789]
25. Paravastu AK, Leapman RD, Yau WM, Tycko R. Molecular structural basis for polymorphism in Alzheimer's β-amyloid fibrils. Proc. Natl. Acad. Sci. USA. 2008; 105:18349–18354. [PubMed: 19015532]
26. Chen X, Hui L, Geiger NH, Haughey NJ, Geiger JD. Endolysosome involvement in HIV-1 Tat-induced neuronal amyloid beta production. Neurobiol. Aging. 2013; 34:2370–2378. [PubMed: 23673310]
27. Daily A, Nath A, Hersh LB. Tat peptides inhibit neprilysin. J. Neurovirol. 2006; 12:153–160. [PubMed: 16877296]
28. Chen Y, et al. HIV-1 Tat regulates occluding and Aβ transfer receptor expression in brain endothelial cells via Rho/ROCK signaling pathway. Oxid. Med. Cell. Longev. 2016:4196572. [PubMed: 27563375]
29. Jeang KT, Xiao H, Rich EA. Multifaceted activities of the HIV-1 transactivator of transcription, Tat. J. Biol. Chem. 1999; 274:28837–28840. [PubMed: 10506122]
30. Garcia JA, Harrich D, Pearson L, Mitsuyasu R, Gaynor RB. Functional domains required for **tat**-induced transcriptional activation of the HIV-1 long terminal repeat. EMBO J. 1988; 7:3143–3147. [PubMed: 3181132]
31. Pierleoni R, et al. Effect of the redox state on HIV-1 tat protein multimerization and cell internalization and trafficking. Mol. Cell. Biochem. 2010; 345:105–118. [PubMed: 20721684]
32. Lara C, Adamcik J, Jordens S, Mezzenga R. General self-assembly mechanism converting hydrolyzed globular proteins into giant multistranded amyloid ribbons. Biomacromolecules. 2011; 12:1868–1875. [PubMed: 21466236]
33. Adamcik J, et al. Microtubule-binding R3 fragment from Tau self-assembles into giant multistranded amyloid ribbons. Angew. Chem. Int. Ed. 2016; 55:618–622.
34. Adamcik J, Mezzenga R. Adjustable twisting periodic pitch of amyloid fibrils. Soft Matter. 2011; 7:5437–5443.
35. Magnuson DS, Knudsen BE, Geiger JD, Brownstone RM, Nath A. Human immunodeficiency virus type 1 tat activates non-N-methyl-D-aspartate excitatory amino acid receptors and causes neurotoxicity. Ann. Neurol. 1995; 37:373–380. [PubMed: 7695237]
36. Nath A, et al. Synergistic neurotoxicity by human immunodeficiency virus proteins Tat and gp120: protection by memantine. Ann. Neurol. 2000; 47:186–194. [PubMed: 10665489]
37. Adamcik J, et al. Understanding amyloid aggregation by statistical analysis of atomic force microscopy images. Nat. Nanotechnol. 2010; 5:423–428. [PubMed: 20383125]
38. Adamcik J, et al. Measurement of intrinsic properties of amyloid fibrils by the peak force QNM method. Nanoscale. 2012; 4:4426–4429. [PubMed: 22688679]
39. Usov I, Mezzenga R. Correlation between nanomechanics and polymorphic conformations in amyloid fibrils. ACS Nano. 2014; 8:11035–11041. [PubMed: 25275956]
40. Milanesi L, et al. Direct three-dimensional visualization of membrane disruption by amyloid fibrils. Proc. Natl. Acad. Sci. USA. 2012; 109:20455–20460. [PubMed: 23184970]

41. Fitzpatrick AW, Park ST, Zewail AH. Exceptional rigidity and biomechanics of amyloid revealed by 4D electron microscopy. Proc. Natl. Acad. Sci. USA. 2013; 110:10976–10981. [PubMed: 23784773]
42. Spedden E, Staii C. Neuron biomechanics probed by atomic force microscopy. Int. J. Mol. Sci. 2013; 14:16124–16140. [PubMed: 23921683]
43. Bieschke J, et al. Small-molecule conversion of toxic oligomers to nontoxic β-sheet-rich amyloid fibrils. Nat. Chem. Biol. 2011; 8:93–101. [PubMed: 22101602]
44. Yang DS, Yip CM, Huang TH, Chakrabartty A, Fraser PE. Manipulating the amyloid-β aggregation pathway with chemical chaperones. J. Biol. Chem. 1999; 274:32970–32974. [PubMed: 10551864]
45. Williams AD, et al. Structural properties of Aβ protofibrils stabilized by a small molecule. Proc. Natl. Acad. Sci. USA. 2005; 102:7115–7120. [PubMed: 15883377]
46. Reyes-Barcelo AA, Gonzales-Velasquez FJ, Moss MA. Soluble aggregates of the amyloid-β peptide are trapped by serum albumin to enhance amyloid-β activation of endothelial cells. J. Biol. Eng. 2009; 3:5–13. [PubMed: 19397812]
47. Lee J, et al. Role of the fast kinetics of pyroglutamate-modified amyloid-β oligomers in membrane binding and membrane permeability. Biochemistry. 2014; 53:4707–4717.
48. Tofoleanu F, Buchete NV. Alzheimer Aβ peptide interactions with lipid membranes: fibrils, oligomers and polymorphic amyloid channels. Prion. 2012; 6:339–345. [PubMed: 22874669]
49. Butterfield DA, Sultana R. Methionine-35 of aβ (1–42): importance for oxidative stress in Alzheimer disease. J. Amino Acids. 2011:198430. [PubMed: 22312456]
50. Jana A, Pahan K. Fibrillar amyloid-beta-activated human astroglia kill primary human neurons via neutral sphingomyelinase: implications for Alzheimer's disease. J. Neurosci. 2010; 30:12676–12689. [PubMed: 20861373]
51. Hategan A, Sengupta K, Kahn S, Sackmann E, Discher DE. Topographical pattern dynamics in passive adhesion of cell membranes. Biophys. J. 2004; 87:3547–3560. [PubMed: 15339814]
52. Nardi J, Bruinsma R, Sackmann E. Adhesion induced reorganization of charged fluid membranes. Phys. Rev. E. 1998; 58:6340–6354.
53. Hategan A, Law R, Kahn S, Discher DE. Adhesively-tensed cell membranes: lysis kinetics and atomic force microscopy probing. Biophys J. 2003; 85:2746–2759. [PubMed: 14507737]
54. Mishra A, Gordon VD, Yang L, Coridan R, Wong GC. HIV Tat forms pores in membranes by inducing saddle-splay curvature: potential role of bidentate hydrogen bonding. Angew. Chem. Int. Ed. 2008; 47:2986–2989.
55. Gupta B, Levchenko TS, Torchilin VP. Intracellular delivery of large molecules and small particles by cell-penetrating proteins and peptides. Adv. Drug Deliv. Rev. 2005; 57:637–651. [PubMed: 15722168]
56. Farago O. Membrane fluctuations near a plane rigid surface. Phys. Rev. E Stat. Nonlin. Soft Matter Phys. 2008; 78:051919. [PubMed: 19113167]
57. Hudson L, et al. Detection of the human immunodeficiency virus regulatory protein Tat in CNS tissues. J. Neurovirol. 2000; 6:145–155. [PubMed: 10822328]
58. Wood SJ, Maleeff B, Hart T, Wetzel R. Physical, morphological and functional differences between pH 5.8 and 7.4 aggregates of the Alzheimer's amyloid peptide Aβ. J.Mol. Biol. 1996; 256:870–877. [PubMed: 8601838]

METHODS-ONLY REFERENCES

59. Li G, Li W, Mumper RJ, Nath A. Molecular mechanisms in the dramatic enhancement of HIV-1 Tat transduction by cationic liposomes. FASEB J. 2012; 26:2824–2834. [PubMed: 22447980]
60. Hollman AM, et al. Selective isolation and purification of tat protein via affinity membrane separation. Biotechnol Prog. 2005; 21:451–459. [PubMed: 15801785]
61. Ban T, Goto Y. Direct observation of amyloid growth monitored by total internal reflection fluorescence microscopy. Methods Enzymol. 2006; 413:91–102. [PubMed: 17046392]

62. Haughey NJ, et al. Perturbation of sphingolipid metabolism and ceramide production in HIV-dementia. Ann Neurol. 2004; 55:257–267. [PubMed: 14755730]

63. Jankowsky JL, Xu G, Fromholt D, Gonzales V, Borchelt DR. Environmental enrichment exacerbates amyloid plaque formation in a transgenic mouse model of Alzheimer disease. J. Neuropathol. Exp. Neurol. 2003; 62:1220–1227. [PubMed: 14692698]

64. Paxinos, G., Franklin, KBJ. The mouse brain in stereotaxic coordinates, Compact. 2nd. Amsterdam: Elsevier Academic Press; 2004.

65. Rockenstein E, Mallory M, Mante M, Sisk A, Masliah E. Early formation of mature amyloid-beta protein deposits in a mutant APP transgenic model depends on levels of Abeta (1–42). J. Neurosci. Res. 2001; 66:573–582. [PubMed: 11746377]

66. Havas D, et al. A longitudinal study of behavioral deficits in an AβPP transgenic mouse model of Alzheimer's disease. J. Alzheimers Dis. 2011; 25:231–243. [PubMed: 21403389]

67. Fields JA, et al. Mechanisms of HIV-1 Tat neurotoxicity via CDK5 translocation and hyper-activation: role in HIV-associated neurocognitive disorders. Curr HIV Res. 2015; 13:43–54. [PubMed: 25760044]

68. Jones TA, Zou J-Y, Cowan SW, Kjeldgaard M. Improved methods for the building of protein models in electron density maps and the location of errors in these models. Acta Crystallographica. 1991; A47:110–119.

69. Lu JX, et al. Molecular structure of β-amyloid fibrils in Alzheimer's disease brain tissue. Cell. 2013; 154:1257–1268. [PubMed: 24034249]

70. Alred EJ, Phillips M, Berhanu WM, Hansmann UM. On the lack of polymorphism in Aβ-peptide aggregates derived from patient brains. Protein Science. 2015; 24:923–935. [PubMed: 25739352]

71. Yang J, et al. The I-TASSER suite: protein structure and function prediction. Nat. Methods. 2015; 12:7–8. [PubMed: 25549265]

72. Kozakov D, et al. How good is automated protein docking? Proteins. 2013; 81:2159–2166. [PubMed: 23996272]

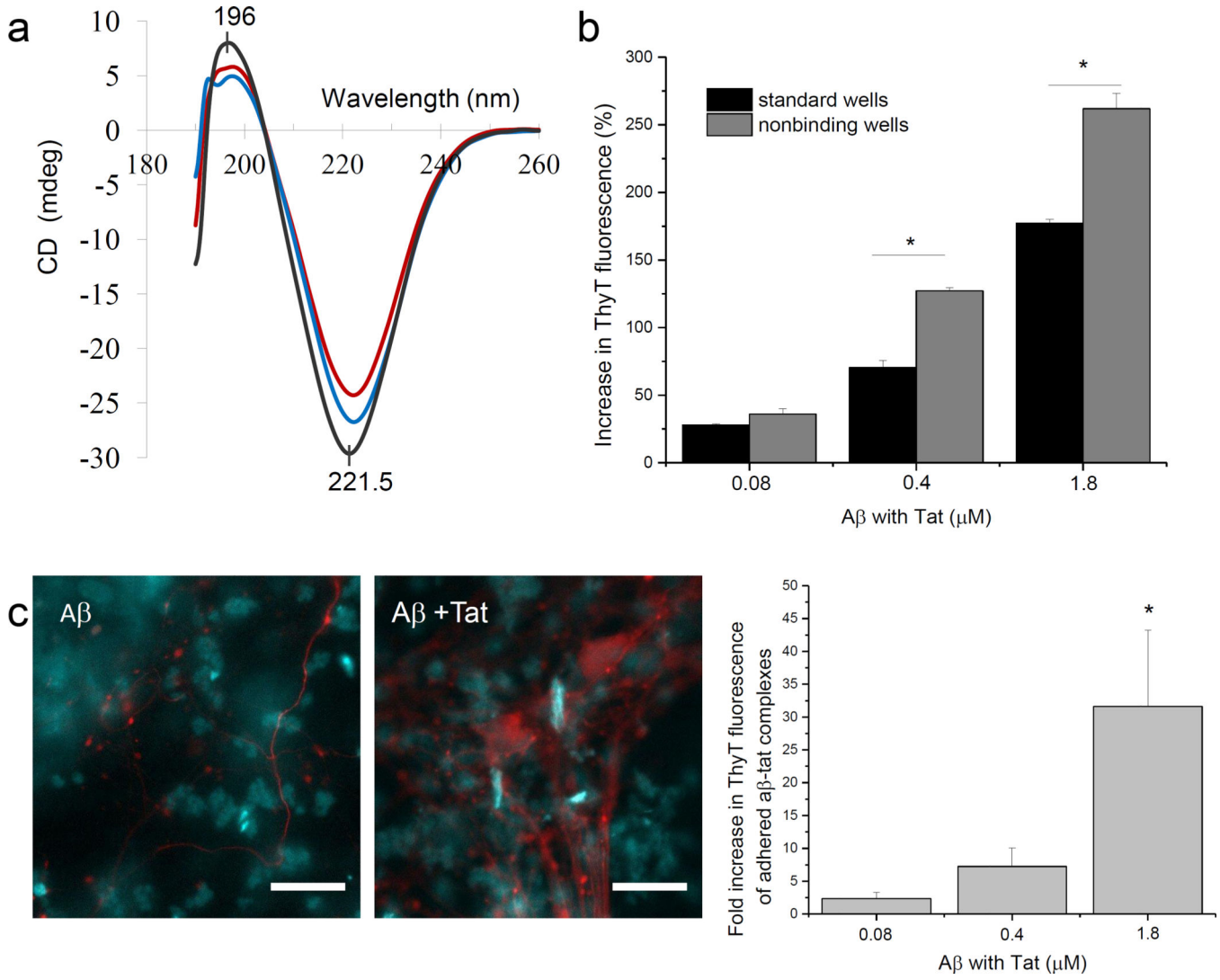

Figure 1. Tat protein increases aggregation and adherence of Aβ fibrils

a) Typical far UV CD spectra shown for 200 μM Aβ (red trace), 200 μM Aβ/0.4 μM Tat (blue trace) and 200 μM Aβ/1.8 μM Tat (black trace) (each an average of 3 traces) indicate that the predominant structure in Aβ fibrils is the β sheet, which increases in the presence of Tat. b) ThyT bulk fluorescence shows increase in aggregation due to Tat and adhesion to surfaces of Aβ–Tat complexes. Data represents mean+ SEM of two independent experiments done with five technical replicates (first experiment) and seven technical replicates (second experiment) and analyzed by unpaired Student's T test: *p<0.05. c) ThyT labeled Aβ and Aβ-Tat structures (cyan color) adhered to neuronal cells in culture. The Aβ-Tat samples show larger aggregates attached to the cells. The neuronal connections within neurons appear red due to labeling of tubulin fibers with tdTomato. Scale bars represent 30 μm. The exposure times and display range in the color channels of the merged images are the same for both images. The graph shows the fold increase in the size of the aggregates attached to the cells. Data represents mean +SEM of 49 (Aβ with 0.08 μM Tat), 31 (Aβ with 0.4 μM Tat), and 25 (Aβ with 1.8 μM Tat) complexes, representative of three independent

experiments. Data was analyzed by ANOVA with Fisher's means comparison test: *$p<0.0001$.

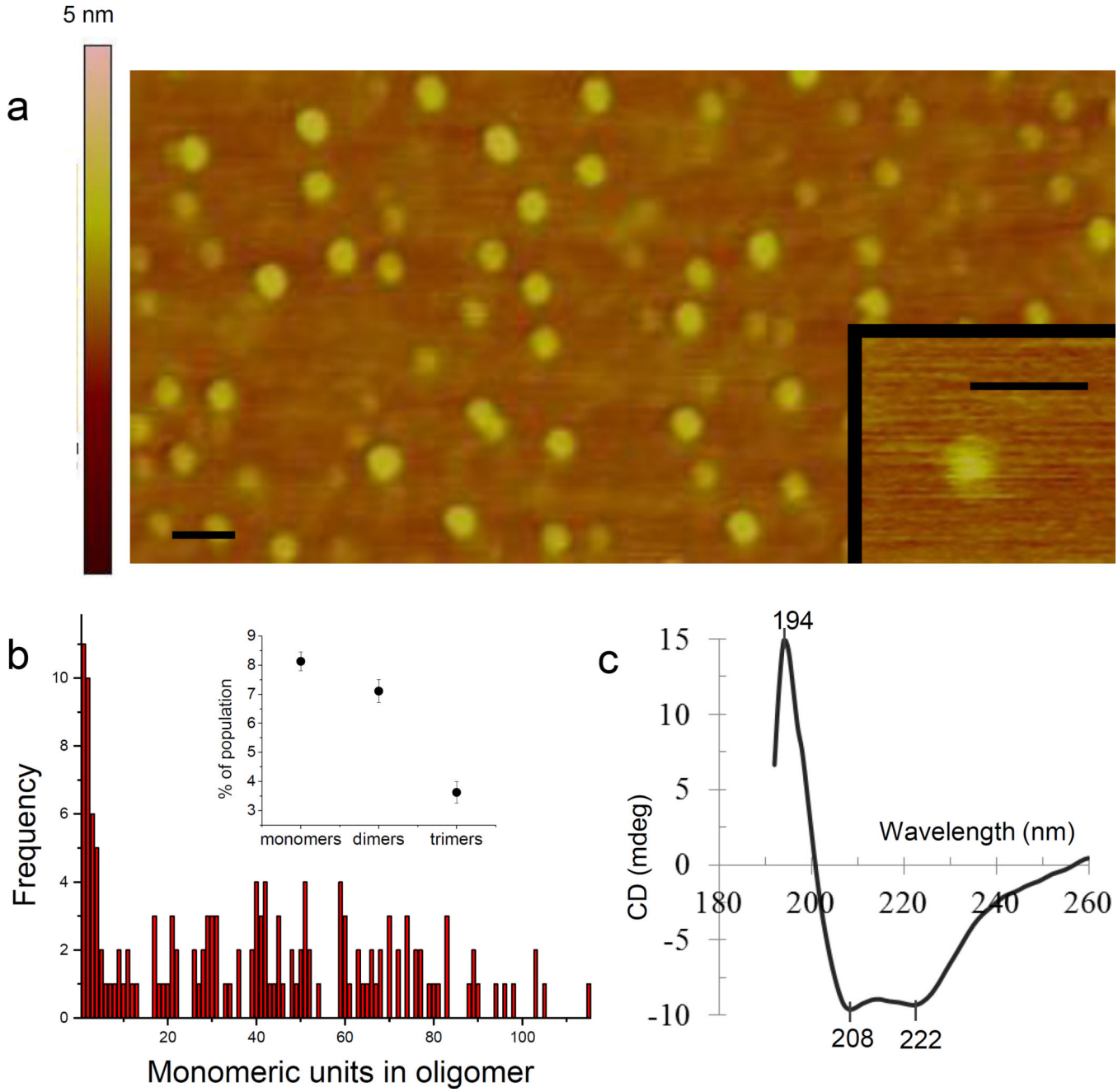

Figure 2. Structure of Tat protein

a) AFM topography image of Tat protein as absorbed from a phosphate buffered saline solution at pH 7.4, onto a clean, atomic flat mica surface, shows a large distribution of sizes, ranging from monomers to large oligomers, all presenting globular structure. Scale bar is 50 nm. Insert represents an experimental zoom-in showing a Tat monomer. Scale bar is 20 nm. b) The distribution of sizes for Tat shows that the most frequent structures are monomers, dimers and small oligomers, however 40–50-mers and larger are present in smaller amounts. The data was derived from 150 particles analysed, representative for 3 technical replicates. Insert shows the relative percentage of monomers, dimers and trimers of Tat, from three

technical replicates with 139, 150, and 543 particles analysed respectively. c) Far-UV CD spectra of 10 μM Tat in PBS solution at pH 7.4 indicates the presence of α-helical structure. The CD spectra presented is an average of 3 traces and has similar shape with spectra of three independent experiments at 20 μM, 1 μM and 0.1 μM concentrations.

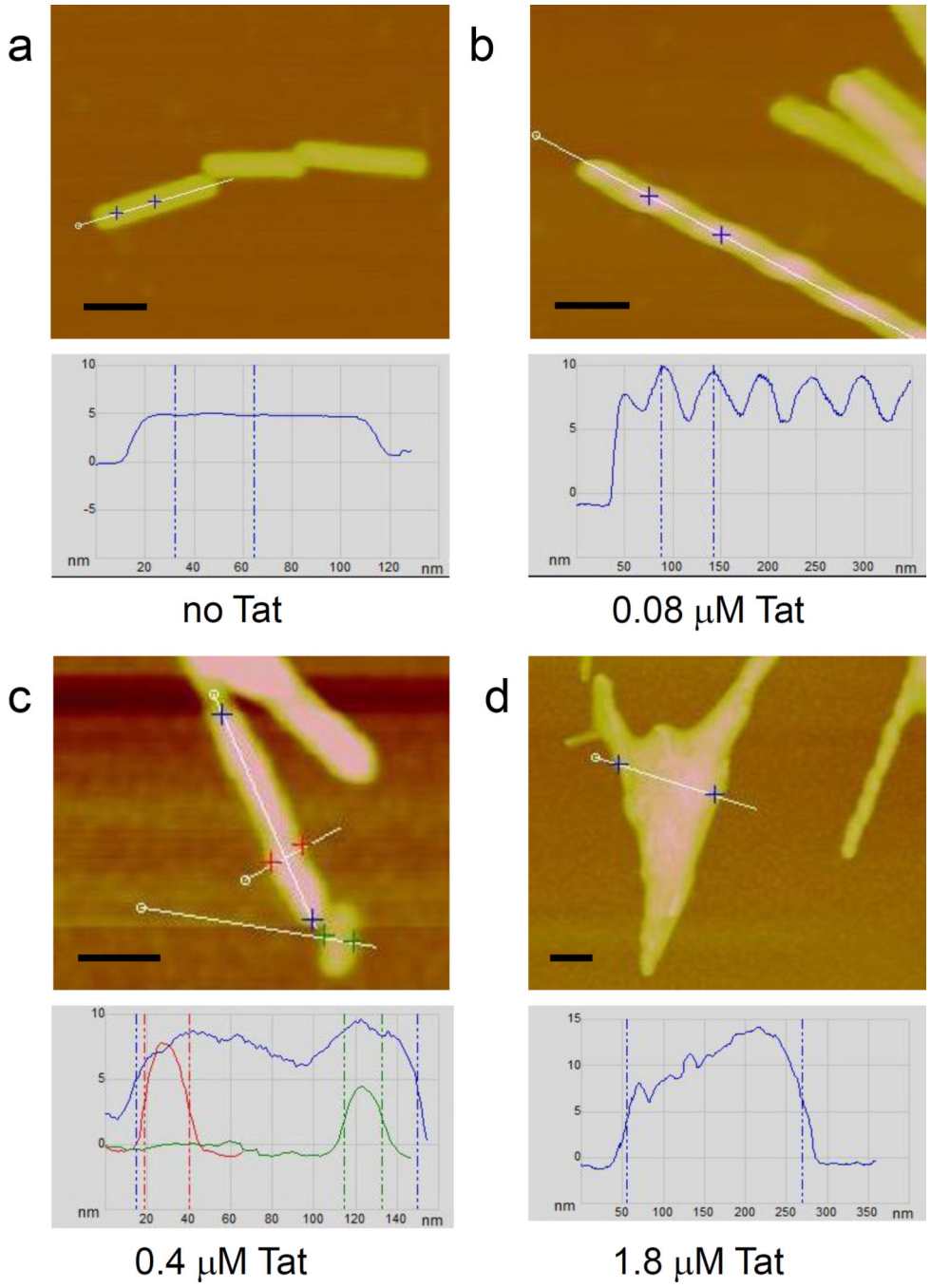

Figure 3. Changes in the Aβ fibril structure induced by Tat protein

Typical AFM topography images of Aβ fibrils in the presence of various concentrations of Tat protein show that the predominant structure observed is a) a typical Aβ fibril, uniform along length, as seen in the graph below, b) a twisted fibrillar structure with 0.08 μM Tat, c) a thick fibril with irregular length and width with 0.4 μM Tat and d) large aggregated patches with 1.8 μM Tat. The graphs represent sections along and across the fibrils shown in the images, at the locations indicated with lines in the corresponding topography image. Scale bars represent 50 nm.

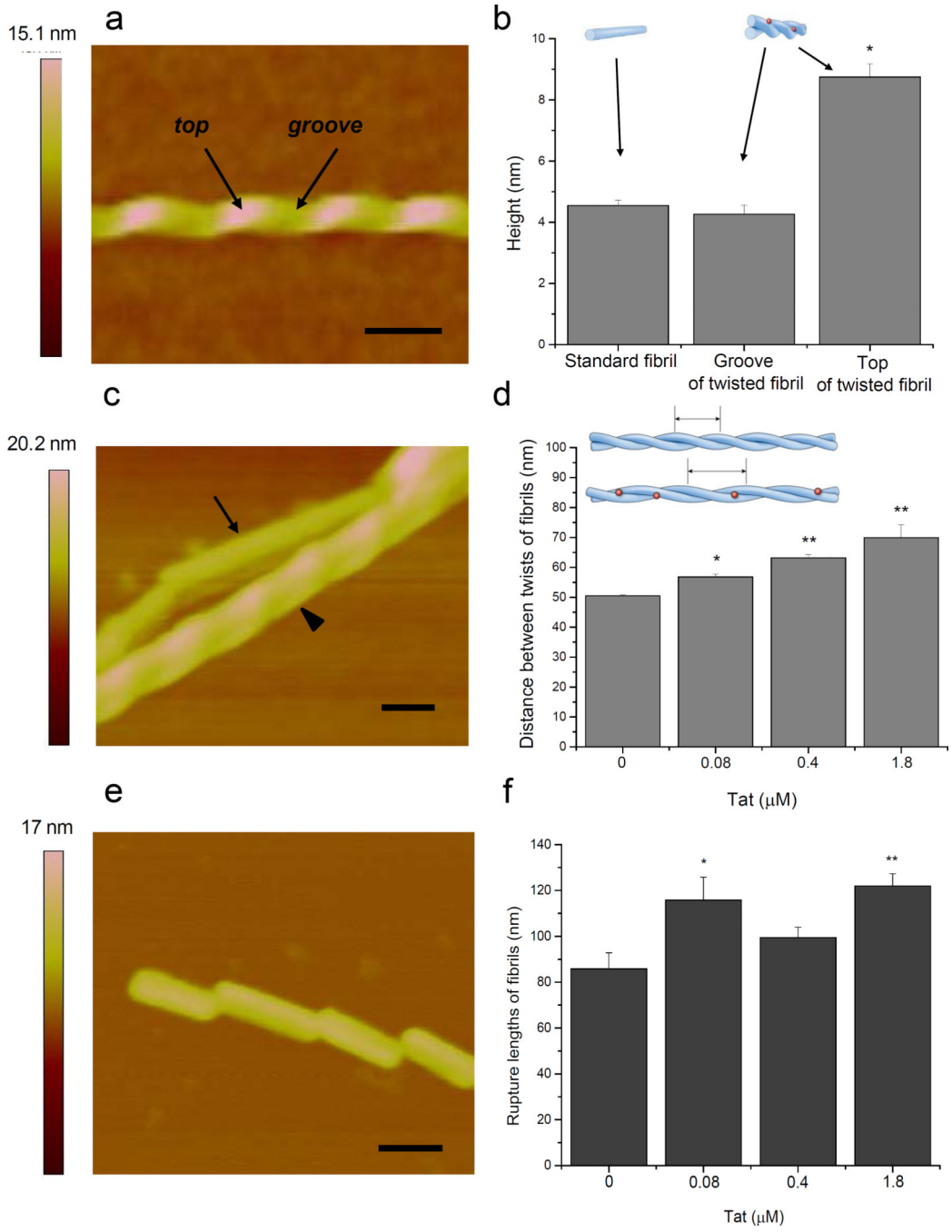

Figure 4. Aβ fibrils untwist and become more mechanically resistant in the presence of Tat

a) An AFM topography image of a typical twisted Aβ fibrillar structure. b) The height at the top of the twist is about twice the height in the groove, and the groove is about the same height as a singular fibril, which shows that two single fibrils are twisted together to give the twisted fibrillar structure. Data represents mean heights + SEM of 21 twists of 7 fibrils and 22 standard fibrils from the Aβ with 0.4 μM Tat sample; *p<1E-6 and there are no significant differences between the height of the grooves and the height of singular fibrils. Similar groove/top and regular fibril height rapports were obtained for the twisted fibrils at

all Tat concentrations (not shown). c) A single fibril (arrow) adjacent to a double twisted fibril (arrow head) in the same topography image. d) The distance between twists in these double fibrils increases significantly with Tat concentration, showing that the fibrils untwist due to Tat. Data represents mean + SEM of 18 (Aβ), 50 (Aβ with 0.08 μM Tat), 54 (Aβ with 0.4 μM Tat), and 19 fibrils (Aβ with 1.8 μM Tat) from two independent experiments: *$p<0.05$ and **$p<0.001$. e) An AFM topography image of a single Aβ fibril that ruptured under air flow during the drying procedure. f) With increasing Tat concentration, the rupture lengths of single fibrils grow significantly, indicating increased mechanical resistance. Data represents mean + SEM for 21 (Aβ), 30 (Aβ with 0.08 μM Tat), 70 (Aβ with 0.4 μM Tat), 53 rupture lengths of fibrils (Aβ with 1.8 μM Tat) from two independent experiments: *$p<0.05$ and **$p<0.001$. All data was analyzed by ANOVA with Fisher's means comparison test. Scale bars represent 50 nm.

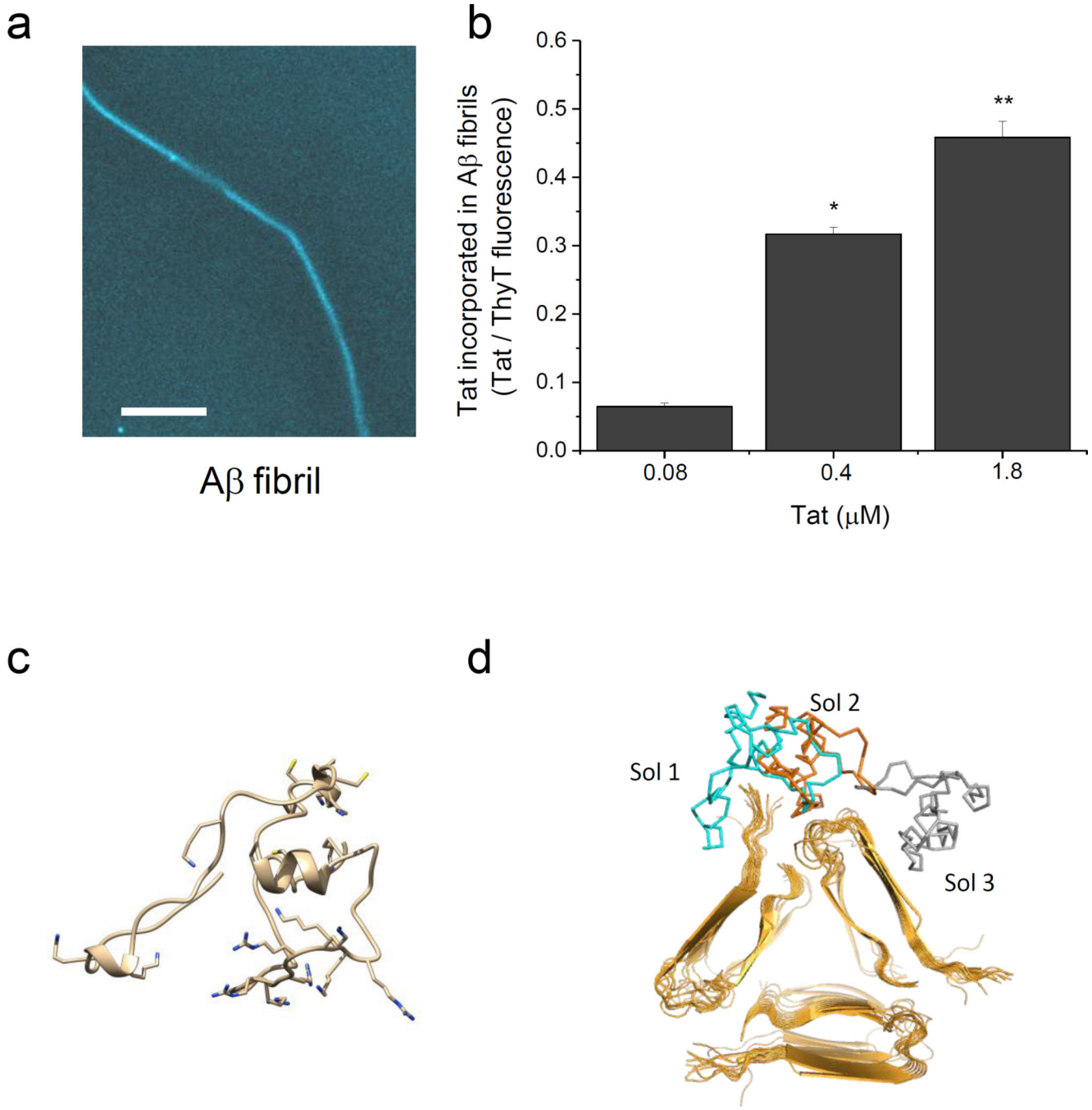

Figure 5. Tat is binding to the external surface of Aβ fibril

a) An Aβ fibril labeled with ThyT. Scale bar is 10 μm. b) The presence of fluorescent Tat in the Aβ fibrils increases in a dose-dependent manner with Tat present at incubation. Data represents mean + SEM for 15 (Aβ with 0.08 μM Tat), 19 (Aβ with 0.4 μM Tat) and 17 fibrils (Aβ with 1.8 μM Tat), from two independent experiments and was analyzed by ANOVA with Fisher's means comparison test: *p<0.001 and **p<1E-6. (c–d) Computer modeling of Aβ–Tat interaction visualizes the surface binding of Tat to the Aβ fibril: The *ab-initio* model of Tat B 1–72 generated by I-Tasser using the crystallographic known

structure of Tat B 1–48[19] as template (c) was docked to the Aβ fibril backbone (golden), which was constructed by repeating the "3 hairpin" structure[25] of Aβ fibril, the result being obtained with ClusPro (d). The first three most probable, low energy, independent conformations were superimposed in the same image (d). The view is in cross-section of fibril. The simulation indicates that Tat binds to the external side at the junction between the hairpins terminals and their turns, allowing in this way further interaction for the bound Tat, due to the external residues, not involved in the binding. Hybrid Tat is presented in (c) in cartoon representation and in (d) as Cα trace, colored blue – the first scored solution, red – the second and grey – the third. The side chains of Lys and Arg residues are represented as sticks with the nitrogen atoms colored blue.

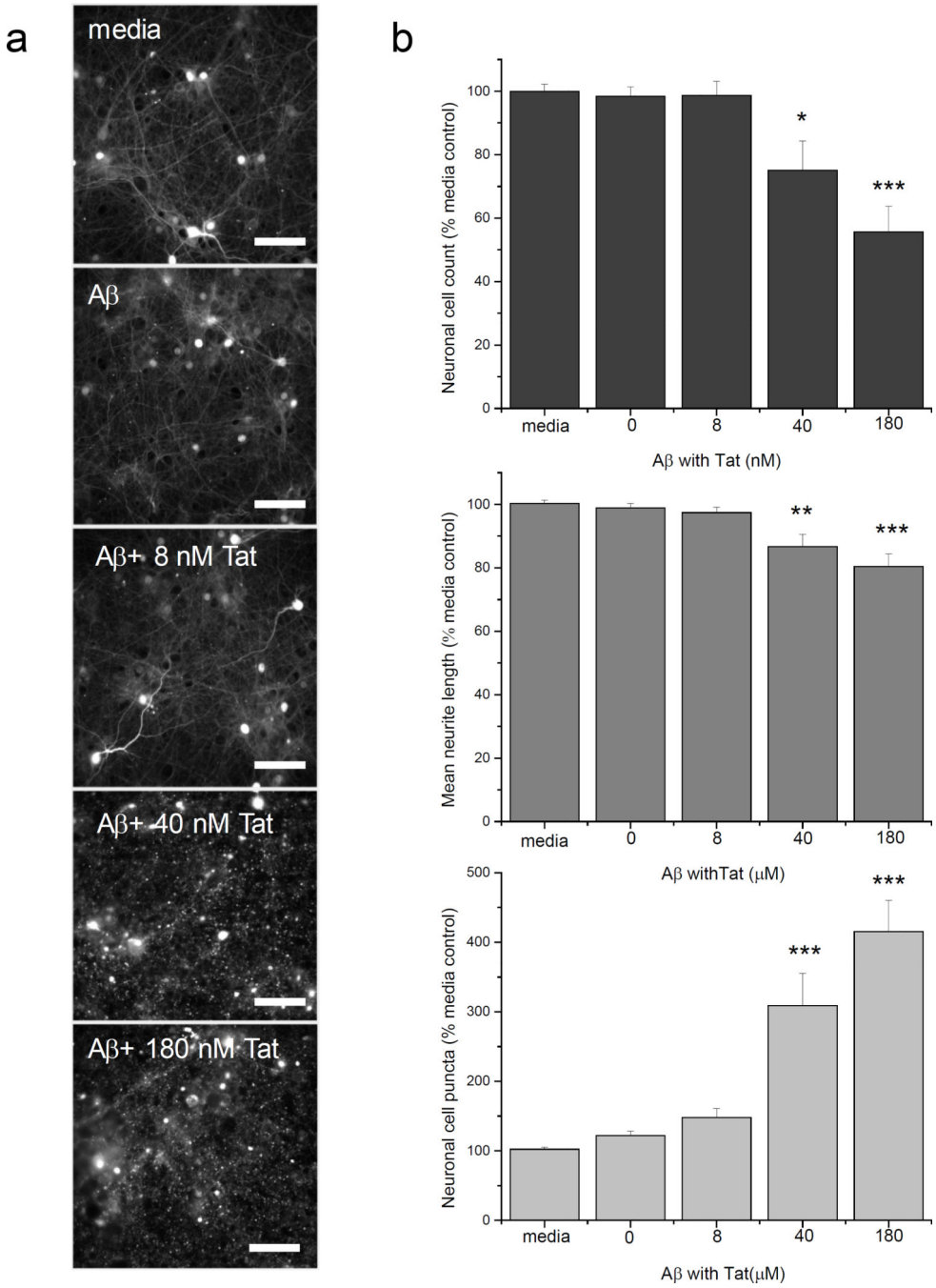

Figure 6. Aβ–Tat complexes show synergistic neurotoxicity in cultured neurons

a) Fluorescence images showing rat neuronal cell cultures where tubulin is fluorescently labeled with td-Tomato fusion protein. Cultures were exposed to the Aβ - Tat complexes and images show the changes after 48 hours of exposure. Aβ - Tat complexes were formed at 200 μM Aβ with varying concentrations of Tat (0.08 μM, 0.4 μM and 1.8 μM). The complexes were automatically diluted 10 fold when incubated with the neurons. Final concentrations are presented in the graphs. Damage to neurons is evident by formation of punctae along neurites. Scale bars are 300 μm. b) Tat in the Aβ -Tat complexes, causes

neuronal damage in a dose-dependent manner leading to decreased neuronal cell counts and retraction of neurite in the remaining neurons. Data represents mean + SEM for 12 images per media sample and 6 images at each dose and is representative of four independent experiments. Analysis was done by ANOVA with Fisher's means comparison test: *$p<0.01$, **$p<0.001$ and ***$p<1E-6$.

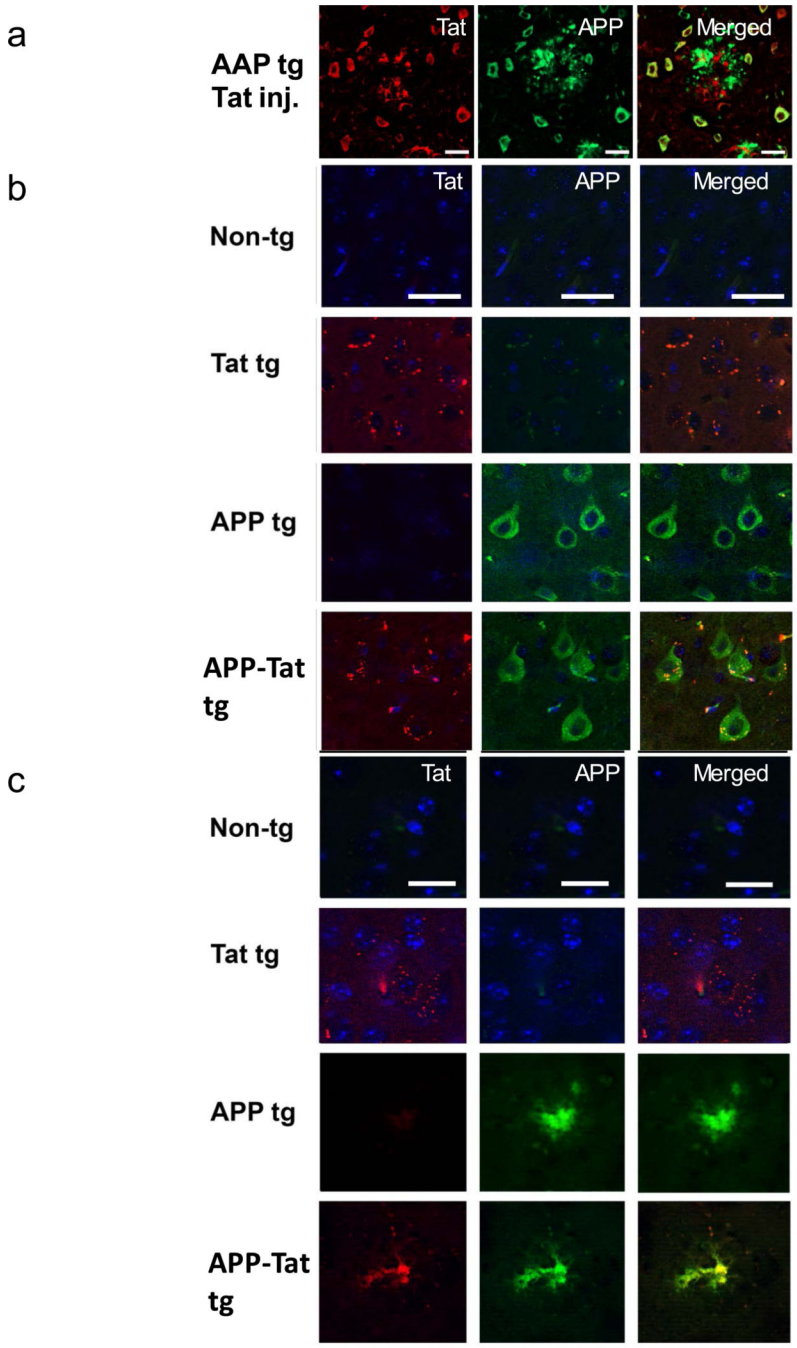

Figure 7. Formation of Aβ-Tat complexes in vivo

a) Tat injected in mice brains colocalizes with amyloid precursor protein (APP) in APP-PS1 transgenic mice. The brain slices were fixed and immunostained for Tat (red) and APP (green) to show their colocalization. b–c) Tat colocalizes with APP in the brains of APP-Tat double transgenic mice, both inside the neurons, mainly in the granular structures (b) and outside of the neuronal cells (c). Free floating vibratome sections from non-transgenic (n=8), Tat transgenic (n=4), APP transgenic (n=4) and APP/Tat transgenic mice (n=8) age 4–6 months were studied. As shown, in the non-transgenic mice no reactivity was detected, in

the Tat transgenic mice immunopositive punctae were detected in association with glial cells, in the APP transgenic mice no Tat reactivity was detected but Aβ plaques were identified in the neocortex and hippocampus. In the APP-Tat transgenic mice plaques displayed co-localization between Tat and Aβ. In (b) and (c) the labeling is with DAPI for cell nuclei, imunostained for Tat (red) and for APP (green). Scale bars are 20 μm for confocal fluorescence images in (a),(b) and (c).

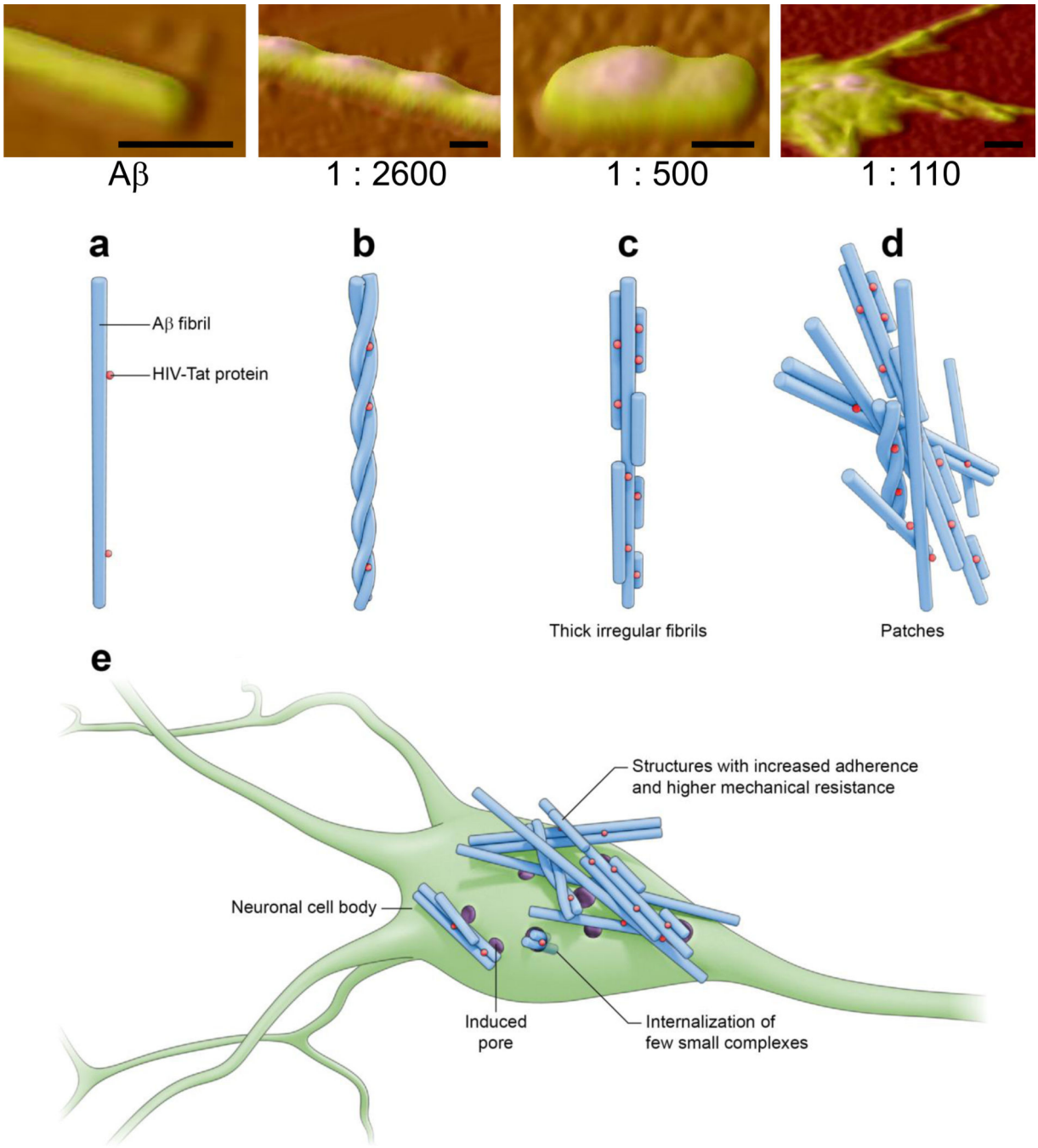

Figure 8. Proposed model of Aβ–Tat interaction and their increased neurotoxicity

a) Tat attaches on the surface of the typical amyloid β fibril. b) At small concentrations, (Tat:Aβ ratio = 1: 2500), the fibrils that randomly come close to each other attach due to Tat and twist around each other to form the double fibril. c) At a 1:500 molar ratio, due to more Tat present, more fibrils, long and small, attach to each other to form the irregular fibrils. d) At a 1:110 molar ratio large patches appear as many fibrils attach to each other. e) These structures are more rigid and have increased adherence due to Tat presence, therefore are binding stronger to the neuronal cell membrane and can induce, only from a mechanical

perspective, pore formation. As a minor pathway, being a trans-membrane penetrating molecule, Tat attached to small aggregates is likely to succeed entering the cells with the Aβ "cargo" to induce damage, in the case of the few small Aβ–Tat aggregates present. Scale bars in a-d AFM tridimensional topography images are 50 nm.